

Effect of disorder on Berry curvature and quantum metric in two-band gapped graphene

Ze Liu^{1,*}, Zhi-Fan Zhang^{1,*}, Zhen-Gang Zhu^{1,2,3,†} and Gang Su^{3‡}

¹ School of Physical Sciences, University of Chinese Academy of Sciences, Beijing 100049, China.

² School of Electronic, Electrical and Communication Engineering, University of Chinese Academy of Sciences, Beijing 100049, China.

³ Kavli Institute for Theoretical Sciences, University of Chinese Academy of Sciences, Beijing 100190, China.

(Dated: April 23, 2024)

The geometric properties of parameter space are mostly described by Berry curvature and quantum metric, which is the imaginary and real part of quantum geometric tensor, respectively. In this work, we calculate the dressed Berry curvature and quantum metric containing eight Feynman diagrams, which is proportional to the leading-order of the concentration of impurities. For a two-band gapped graphene model, we find the disorder does not break the original symmetry of Berry curvature and quantum metric but decrease (increase) the absolute value of conductor (valence) band. We show how impurities affect the Berry curvature and quantum metric, laying the foundation for the study of the influence of impurities on the electron transport properties.

I. INTRODUCTION

As the frontier of condensed matter physics, the geometric properties of quantum states are of great significance in many areas. One of the most general description of the evolution of a cell-periodic Bloch state under the variation of a vector parameter \mathbf{k} is the quantum geometric tensor (QGT) proposed by Provost and Vallee¹. Its imaginary (anti-symmetric) part is Berry curvature (BC), a quantity manifested in many transport properties and observed in many materials, which can be regarded as an emergent gauge field in the parameter space²⁻⁴. Moreover, the integrated of BC over the momentum space leads to the famous quantum number in quantum Hall effect and Chern insulator⁵⁻¹⁰, and in nonlinear response¹¹⁻²⁰, and so on. The quantum metric (QM), the real (symmetric) part of QGT, is another important geometric quantity²¹⁻²⁶. Very recently, many physical phenomena related to QM²⁷⁻³³ have been proposed. As an illustration, Chen and Law establish a Ginzburg-Landau theory from a microscopic flat-band Hamiltonian to show that the superconducting coherence length is determined directly by the QM²⁷. Furthermore, some experiments have been conducted intending to confirm the nonlinear quantum transports induced by the QM³⁴⁻³⁶. Generally speaking, the BC and QM are both fundamental quantities for understanding many new topological effects, either known or unknown.

The BC and QM reflect the topology of many-particle systems and regulate particles' dynamics. Thus a quite fundamental question may raise whether the dynamical properties and many-body interaction can mutually modify the topological properties of the system. To be more specific, a precise discussion how the interaction affects BC and QM is urgently needed. Intriguingly, Wei Chen has provided a formalism for the BC and QM³⁷, which are applicable to realistic gapped materials at finite temperature and in the presence of many-body interactions. They introduce the spectral functions to characterize the BC and QM, and discuss how many-body interactions in-

fluence the shape of these spectral functions. Nevertheless, they obtain the leading order of impurity scattering which does not contribute to the QM or BC in the Chern insulator because the integral of the spectral function is equal to zero. From another point of view, numerous theoretical and experimental results have proved that impurities can affect electron transport³⁸⁻⁴⁵. As quantum transport is very closely related to the BC and QM, the role of disorder on them should be explored.

In this work, we study this topic using eight Feynman diagrams containing the first-order contributions of the impurity with the help of the first Born approximation (FBA) and vertex correction. We specifically study a two-band gapped graphene model, and find that the disorder contribute a certain correction, named as dressed BC and QM. Our calculation and results provide crucial information for understanding the influence of impurity interaction on BC and QM. Meanwhile, it is also a solid foundation to further explore the contribution of impurities on geometric quantities.

The structure of this paper is organized as follows. In Sec. II, we present the definition and relations of QGT, BC and QM in the zero temperature and non-interaction limit and introduce the dressed BC and QM with many body interactions at finite temperatures. In Sec. III, we give the eight Feynman diagrams about side jump scattering to explain how to calculate the effect of disorder using the FBA and vertex correction. Next we discuss the results in a two-band gapped graphene model in Sec. IV. Finally we summarize and discuss our results in Sec. V.

II. QUANTUM GEOMETRIC TENSOR

The QGT of n -th band in the \mathbf{k} space can be written as $T_{\mathbf{k}}^n$, whose imaginary (anti-symmetric) part is Berry curvature (BC), $\Omega_{\mu\nu,\mathbf{k}}^n = -2\text{Im}T_{\mu\nu,\mathbf{k}}^n$, and real (symmetric)

part is quantum metric (QM) tensor, $g_{\mu\nu,\mathbf{k}}^n = \text{Re}T_{\mu\nu,\mathbf{k}}^n$ ²⁹,

$$T_{\mu\nu,\mathbf{k}}^n = \langle \partial_\mu u_{\mathbf{k}}^n | 1 - \mathcal{P}^n(\mathbf{k}) | \partial_\nu u_{\mathbf{k}}^n \rangle = g_{\mu\nu,\mathbf{k}}^n + i \frac{\Omega_{\mu\nu,\mathbf{k}}^n}{2}, \quad (1)$$

where $\mu, \nu \in (x, y, z)$, $\partial_\mu = \partial_{k^\mu}$, $\mathcal{P}^n(\mathbf{k}) = |u_{\mathbf{k}}^n\rangle\langle u_{\mathbf{k}}^n|$ is the projector on the band n and the quantum metric characterizes a distance in Hilbert space, defined as

$$ds^{2,n} = 1 - |\langle u_{\mathbf{k}}^n | u_{\mathbf{k}+\mathbf{d}\mathbf{k}}^n \rangle|^2 = g_{\mu\nu,\mathbf{k}}^n dk^\mu dk^\nu, \quad (2)$$

and the Berry curvature tensor is a gauge-field tensor derived from the Berry vector potential, $\mathcal{A}_{\mathbf{k}}^n = i\langle u_{\mathbf{k}}^n | \nabla_{\mathbf{k}} | u_{\mathbf{k}}^n \rangle$, in analogy to electrodynamics^{4,5},

$$\Omega_{\mathbf{k}}^n = \nabla \times \mathcal{A}_{\mathbf{k}}^n. \quad (3)$$

For the sake of discussing many-body interactions perturbatively, the dressed Berry curvature and quantum metric at finite temperature can be proposed using the linear response theory³⁷. Suppose that there is an external electric field E^μ , the corresponding dipole energy can be written as

$$\delta h_{\mathbf{k}} = -iqE^\mu \partial_\mu, \quad (4)$$

where q indicates the charge of the particle. Within the linear response theory we can define a charge polarization operator $U_{\mu,\mathbf{k}}$ and the susceptibility $\chi_{\mu\nu,\mathbf{k}}(i\omega)$ of its average,

$$U_{\mu,\mathbf{k}}^n = \sum_{nn'} \mathcal{A}_{\mu,\mathbf{k}}^n c_{n,\mathbf{k}}^\dagger c_{n',\mathbf{k}} = -U_{\mu,\mathbf{k}}^{n\dagger}, \quad (5)$$

$$\langle U_{\mu,\mathbf{k}}^n(t) \rangle = \chi_{\mu\nu,\mathbf{k}}^n(t) q E^\nu(t),$$

where the driving electric field is $E^\nu(t) = E^\nu e^{-i\omega t}$, and the Matsubara version of the susceptibility is calculated by

$$\chi_{\mu\nu,\mathbf{k}}^n(i\omega) = - \int_0^\beta d\tau e^{i\omega\tau} \langle T_\tau U_{\mu,\mathbf{k}}^n(t) U_{\nu,\mathbf{k}}^{n'}(0) \rangle. \quad (6)$$

Therefore, we can obtain the dressed BC and QM³⁷

$$T_{\mu\nu,\mathbf{k}}^{\text{d},n} = \frac{1}{2\pi} \int_0^\omega [i\chi_{\mu\nu,\mathbf{k}}^n(\omega) - i\chi_{\nu\mu,\mathbf{k}}^{n*}(\omega)] d\omega,$$

$$g_{\mu\nu,\mathbf{k}}^{\text{d},n} = -\frac{1}{2\pi} \int_0^\omega \text{Im} [\chi_{\mu\nu,\mathbf{k}}^n(\omega) + \chi_{\nu\mu,\mathbf{k}}^n(\omega)] d\omega, \quad (7)$$

$$\Omega_{\mu\nu,\mathbf{k}}^{\text{d},n} = -\frac{1}{\pi} \int_0^\omega \text{Re} [\chi_{\mu\nu,\mathbf{k}}^n(\omega) - \chi_{\nu\mu,\mathbf{k}}^n(\omega)] d\omega,$$

where the superscript d indicates these quantities are dressed by impurity scattering.

III. THE EFFECTS OF DISORDER

To study the effects of disorder in detail, we consider an elastic scattering⁴², i.e., $V(\mathbf{r}) = \sigma_0 \sum_i u_i \delta(\mathbf{r} - \mathbf{R}_i)$,

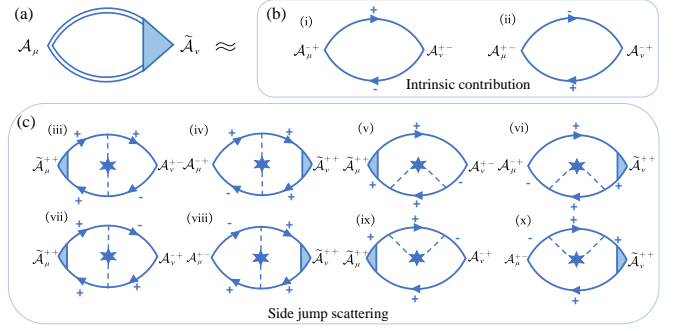


FIG. 1. Feynman diagrams for susceptibility (a). Under FBA and vertex correction, these diagrams are classed into (b) intrinsic contribution and (c) extrinsic side jump scattering. (i) and (iii-vi) are for valence band while (ii) and (vii-x) are for conduction band. The double and single solid lines stand for the full and free-particles Matsubara Green's function, where arrows to the right and left indicate retarded and advanced Green's function, respectively. The Eigen bands of a generic two-band model are labeled as \pm . The dash-star-dashed lines represent the disorder scattering. The light blue shadow represents the corrected vertices.

where the disorder is modeled as δ -function scatters with a random distribution $\{\mathbf{R}_i\}$, u_i indicates the strength of disorder satisfying $\langle u_i \rangle_{\text{imp}} = 0$, $\langle u_i^2 \rangle_{\text{dis}} = u_0^2 \neq 0$, and σ_0 is a unit matrix.

We can draw the Feynman diagrams of the susceptibility $\chi_{\mu\nu,\mathbf{k}}^n(\omega)$ according to Eq. (6), which is a two-particle Green's function with two operators at each of the external vertices⁴⁶ as shown in Fig. 1(a),

$$\chi_{\mu\nu,\mathbf{k}}^n(\omega) = \sum_m \mathcal{A}_{\mu,\mathbf{k}}^{nm} \tilde{\mathcal{A}}_{\nu,\mathbf{k}}^{mn} \frac{1}{\beta} \sum_{ip} \mathcal{G}_{\mathbf{k}}^m(ip + i\omega) \mathcal{G}_{\mathbf{k}}^n(ip), \quad (8)$$

where n, m show different energy bands, $\tilde{\mathcal{A}}_{\nu,\mathbf{k}}^{mn}$ represents the dressed vertices corrected by impurities, which we will discuss below. And $\mathcal{G}_{\mathbf{k}}^n(ip) = \frac{1}{ip - \epsilon_{\mathbf{k}} - \Sigma_{\mathbf{k}}}$ is the full Green's function, where $\Sigma_{\mathbf{k}}$ is the self-energy function for electrons.

According to Eq. (8), we have retained several diagrams of the larger impurity contributions drawn in Fig. 1. Diagrams (b) are intrinsic contributions, not related to the impurity scattering. By expanding the double-line full Green's function with the aid of FBA and dressed vertices, we can obtain eight diagrams [Fig. 1(c)] showing the effect of first-order disorder scattering, in which (iii)-(vi) are for $+$ band and (vii)-(x) are for $-$ band. According to these diagrams, the susceptibility in Eq. (8) can be calculated, and the influence of the impurities on BC and QM can be further studied.

A. The summation on Matsubara frequencies in Feynman diagrams

In order to derive the susceptibility, firstly we need to calculate the summation on Matsubara frequencies

of Green's function in the Feynman diagrams. Following chapter 3 of Mahan⁴⁷, we work with Matsubara frequencies, while allow the evaluation of the integrals with straightforward contour integral techniques. These details are shown in the Appendix A.

B. The self-energy and relaxation time

Further, we need to figure out the self-energy and relaxation time of electrons. Herein, we define the free-particle Green's function is $G(ip) = \frac{1}{ip + i\omega - \varepsilon_{\mathbf{k}}}$ and the Dyson equation for full Green's function \mathcal{G} can be written as $\mathcal{G} = G + G\Sigma\mathcal{G}$. Upon disorder averaging we obtain the self-energy equation⁴⁸

$$\Sigma_{\mathbf{k}} = \langle V \rangle_{\text{imp}} + \langle VGV \rangle_{\text{imp}} + \langle VGVGV \rangle_{\text{imp}} + \dots \quad (9)$$

To get the leading order of disorder, we have

$$\Sigma^{\pm} = \langle V_{\mathbf{k}\mathbf{k}'}^{\pm+} V_{\mathbf{k}'\mathbf{k}}^{\pm\pm} \rangle_{\text{imp}} G^+ + \langle V_{\mathbf{k}\mathbf{k}'}^{\pm-} V_{\mathbf{k}'\mathbf{k}}^{\pm\pm} \rangle_{\text{imp}} G^-, \quad (10)$$

where the eigenstates of a general two-band model are labeled as $n = \pm$ and $V_{\mathbf{k}\mathbf{k}'} = V(\mathbf{k} - \mathbf{k}')$ is the Fourier transform of the single impurity potential. It is noted that we ignore the off-diagonal part of the self-energy because of the translation invariant after the impurity average⁴⁹. Furthermore, the relaxation time can be expressed as

$$\frac{1}{\tau_{\mathbf{k}}} = -\frac{2}{\hbar} \text{Im} \Sigma_{\mathbf{k}}. \quad (11)$$

C. The dressed vertex

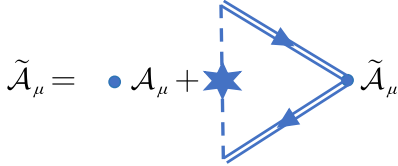


FIG. 2. The Dyson equation for the dressed vertices. The double solid lines stand for the full Matsubara Green's function. The dash-star-dashed line represents the disorder scattering.

Shown in Fig. 2, the Dyson equation for dressed vertices is written as^{46,48}

$$\tilde{\mathcal{A}}_{\mu,\mathbf{k}}^{nn} = \mathcal{A}_{\mu,\mathbf{k}}^{nn} + \sum_{\mathbf{k}'} \langle V_{\mathbf{k}\mathbf{k}'}^{nn} V_{\mathbf{k}'\mathbf{k}}^{nn} \rangle \mathcal{G}_{\mathbf{k}'}^{R,n} \mathcal{G}_{\mathbf{k}'}^{A,n} \tilde{\mathcal{A}}_{\mu,\mathbf{k}'}^{nn}, \quad (12)$$

where the first term free of impurities is the Berry connection without interaction. As we know, in vertex correction, every disorder line that connects retarded and advanced Green's function provides a factor $n_i u_0^2$; while the Green's function product $\mathcal{G}^R \mathcal{G}^A$ is proportional

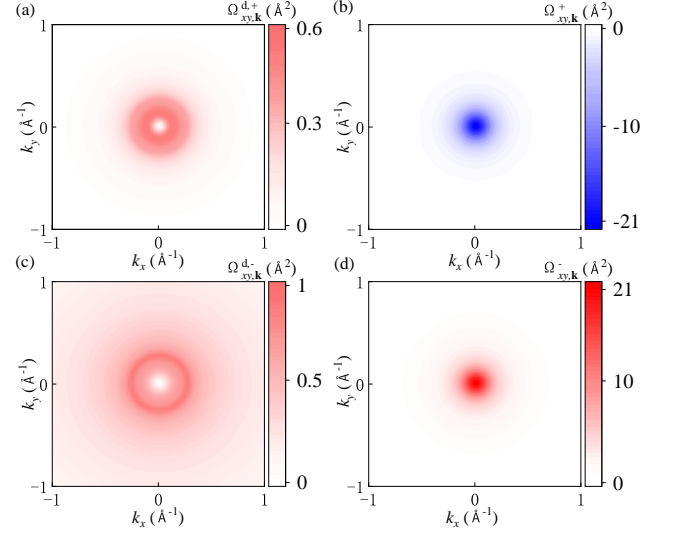


FIG. 3. The 2D contour for off-diagonal component of (a),(c) dressed BC $\Omega_{xy,\mathbf{k}}^d$ and (b),(d) $\Omega_{xy,\mathbf{k}}$ BC. (a)-(b) are for the + band while (c)-(d) are for the - band. The parameters are $\Delta = 2$ eV, $n_i u_0^2 L^2 = 10$ eV²Å², $v_D = 10^6$ m/s, $\varepsilon_f = 2$ eV.

$(n_i u_0^2)^{-1}$. The overall vertex correction is independent of the concentration of impurities n_i . Thus, all the diagrams [Fig. 1(iii)-(x)] are the leading order of the concentration of impurities n_i representing only the side jump scattering. Although higher order effects, i.e. skewing scattering, can also contribute to these geometric quantities, we have neglected them in this work.

IV. TWO-BAND GAPPED GRAPHENE MODEL

To make our discussion more specifically, we consider a two-band gapped graphene model⁵⁰,

$$H = \begin{bmatrix} \frac{\Delta}{2} & v_D \hbar (\tau k_x - i k_y) \\ v_D \hbar (\tau k_x + i k_y) & -\frac{\Delta}{2} \end{bmatrix}, \quad (13)$$

where Δ is the gap, $\tau = \pm 1$ are valley indexes, v_D is the Dirac velocity, and $\varepsilon_{\mathbf{k}}^{\pm} = \pm \sqrt{v_D^2 \hbar^2 \mathbf{k}^2 + (\frac{\Delta}{2})^2}$. The BC is derived

$$\Omega_{xy,\mathbf{k}}^{\pm} = \mp \frac{v_D^2 \hbar^2 \Delta}{4 [v_D^2 \hbar^2 \mathbf{k}^2 + (\Delta/2)^2]^{3/2}}, \quad (14)$$

and the four components of QM are derived as

$$g_{\mu\nu,\mathbf{k}}^{\pm} = \frac{v_D^2 \hbar^2 \{ [v_D^2 \hbar^2 \mathbf{k}^2 + (\Delta/2)^2] \delta_{\mu\nu} - v_D^2 \hbar^2 k_{\mu} k_{\nu} \}}{4 [v_D^2 \hbar^2 \mathbf{k}^2 + (\Delta/2)^2]^2}. \quad (15)$$

Motivated by the above discussions in Eqs. (8)-(12) and considered only the impurity average proportional to the

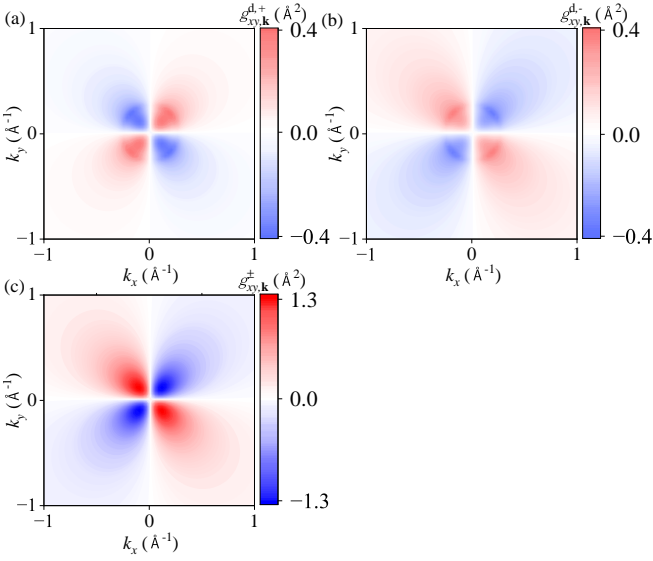


FIG. 4. The 2D contour for off-diagonal component of (a), (b) dressed QM $g_{xy,\mathbf{k}}^d$ and (c) QM $g_{xy,\mathbf{k}}$. (a) is for the + band while (b) is for the - band. The parameters are $\tau = 1$, $\Delta = 2$ eV, $n_i u_0^2 L^2 = 10$ eV $^2 \text{\AA}^2$, $v_D = 10^6$ m/s, $\varepsilon_f = 2$ eV.

leading order of the concentration of impurities n_i , we can get self-energy and relaxation time (see Appendix B1, B2)

$$\Sigma^\pm = -\frac{n_i u_0^2 L^2}{4\pi v_D^2 \hbar^2} \left(\varepsilon_{\mathbf{k}} \pm \frac{\Delta^2}{4\varepsilon_{\mathbf{k}}^+} \right) \left(\ln \left| \frac{\varepsilon^2 - \varepsilon_c^2}{\varepsilon^2} \right| + i\pi \right),$$

$$\frac{1}{\tau_{\mathbf{k}}^\pm} = -\frac{2}{\hbar} \text{Im} \Sigma_{\mathbf{k}}^\pm = \frac{n_i u_0^2 L^2}{2v_D^2 \hbar^3} \left(\varepsilon_{\mathbf{k}}^\pm + \frac{\Delta^2}{4\varepsilon_{\mathbf{k}}^\pm} \right),$$
(16)

where we assume u_i as a constant u_0 , L stands for unit length, and ε_c is the cut-off energy. Thus, the dressed vertex is derived as (see Appendix B3)

$$\tilde{\mathcal{A}}_{\mu,\mathbf{k}}^{++}(\omega) = \frac{1 - B + \frac{\omega^2}{\hbar^2} \tau_{\mathbf{k}}^{+2} + \frac{i\omega}{\hbar} \tau_{\mathbf{k}}^+ B}{(1 - B)^2 + \frac{\omega^2}{\hbar^2} \tau_{\mathbf{k}}^{+2}} \mathcal{A}_{\mu,\mathbf{k}}^{++},$$
(17)

where $B = \frac{n_i u_0^2 L^2}{4\hbar^3 v_D^2} \varepsilon_{\mathbf{k}}^+ \sin^2 \theta_{\mathbf{k}}^+$.

A. The effect of disorder on BC

After tedious steps in Appendix B, we obtain the dressed BC at zero temperature limit in Appendix B5 and present the results in Fig. 4. It is easy to see that dressed BC and BC have the same symmetry, both being a circular in the k_x - k_y plane. This tells us that the impurities scattering does not affect the symmetry of geometric quantity BC in the \mathbf{k} space, although scattering potential energy is angle-dependent. The difference, however, is that the bare BC (no dressing) of conduction (valence) band [Fig. 3(b),(d)] is negative (positive) as a whole, while both the dressed BC of conduction and

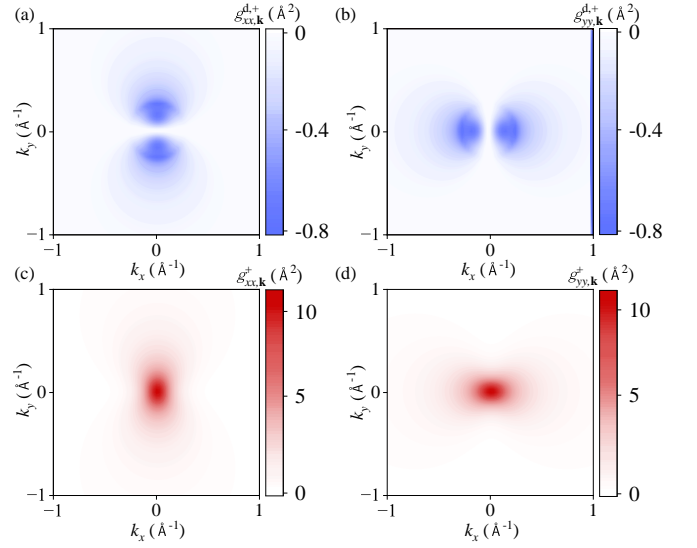


FIG. 5. The 2D contour for diagonal components of (a),(b) dressed QM $g_k^{d,+}$ and (c),(d) QM g_k^+ . (a)(c) are for xx components while (b)(d) are for yy components. The parameters are $\tau = 1$, $\Delta = 2$ eV, $n_i u_0^2 L^2 = 10$ eV $^2 \text{\AA}^2$, $v_D = 10^6$ m/s, $\varepsilon_f = 2$ eV.

valence band [Fig. 3(a),(c)] are positive. Therefore, the scattering will decrease the absolute value of conduction band BC but increase the absolute value of valence band BC. In addition, there are also some differences in trend along the radial between dressed BC and BC. For conduction (valence) band, BC is minimum (maximum) at $k_x = k_y = 0$ and gradually increases (decreases) as $|\mathbf{k}|$ increases. In contrast, dressed BC first increases sharply from $k_x = k_y = 0$ and then decreases gradually with the increase of $|\mathbf{k}|$. Numerically, when impurity $n_i u_0^2 L^2 = 10$ eV $^2 \text{\AA}^2$, the dressed BC is an order of magnitude smaller than bare BC. For diagonal terms, both bare BC and the dressed BC are zero according to Eq. (7).

B. The effect of disorder on QM

Fig. 4 illustrates the two-dimensional (2D) contour plot for the off-diagonal elements of the dressed QM $g_{xy,\mathbf{k}}^{d,+/-}$ and bare QM $g_{xy,\mathbf{k}}^\pm$ (see Appendix B5). It is seen both dressed QM and bare QM are of the same symmetry. There are in each graph two node lines where bare QM is 0, centered at $k_x = k_y = 0$, and crossing through \mathbf{k} space. All of them are symmetric with respect to the vertical mirror along $k_x = k_y$ or $k_x = -k_y$ and anti-symmetric with respect to those along $k_x = 0$ or $k_y = 0$. Interestingly, while the bare QM and the dressed QM for the valence band have a similar distribution, and both are negative in the first and third quadrants and positive in the second and fourth quadrants; while the dressed QM for the conduction band is of opposite sign. It means that the disorder scattering can reduce the absolute value of

QM for the conduction band (+ band) but increase the absolute value of QM for valence band (- band). This result is consistent with BC. It is found that the dressed QM is an order of magnitude smaller than the bare QM.

The diagonal bare QM and dressed QM for conduction band are shown in Fig. 5. All the four quantities, i.e. $g_{xx/yy,\mathbf{k}}^{d,+}$, $g_{xx/yy,\mathbf{k}}^+$ are of two symmetry vertical mirrors along $k_x = 0$ or $k_y = 0$. The difference is that the nodal lines for $g_{xx,\mathbf{k}}^{d,+}$ and $g_{yy,\mathbf{k}}^{d,+}$ lie along $k_y = 0$ and $k_x = 0$, respectively. Another feature is that there are a two-fold axis along k_y and k_x , respectively, for $g_{xx,\mathbf{k}}^{d,+}$ (and $g_{xx,\mathbf{k}}^+$) and $g_{yy,\mathbf{k}}^{d,+}$ (and $g_{yy,\mathbf{k}}^+$). Also, both $g_{xx,\mathbf{k}}^+$ and $g_{xx,\mathbf{k}}^{d,+}$ are extending in the y direction, and both $g_{yy,\mathbf{k}}^+$ and $g_{yy,\mathbf{k}}^{d,+}$ are extending in the x direction. These distributions in momentum space of the xx and yy components of QM look like atomic orbitals of p_x and p_y and probably of the symmetry of p_x and p_y in the momentum space. In other words, the rotation of $g_{xx,\mathbf{k}}^+$ by $\pi/2$ along the k_z axis completely yields $g_{yy,\mathbf{k}}^+$, which is also true for dressed QM. Nevertheless, the maximum value of QM is located at the center of $k_x = k_y = 0$; while dressed QM approaches zero at that point, and the extreme value is located on both side of the original point.

V. CONCLUSION AND DISCUSSION

With the help of FBA and dressed vertices, we calculate the eight Feynman diagrams to show how disorder side-jump scattering affects BC and QM. In the gapped graphene, we find that disorder does not affect the symmetry in \mathbf{k} space but affect the magnitude of BC and QM. Furthermore, impurities may affect some phenomena, which are mainly induced by the BC or QM, such as anomalous Hall effect⁴⁸, nonlinear Hall effect⁴³, etc. Our calculations provide an idea to explain how impurities affect transport, which is expected to be further understood in the future.

In the process of calculation, we only consider all first-order diagrams describing side jump scattering, where

the effect of disorder on BC and QM is about 0.1 times as many as those with non-interaction. As for skew scattering for second-order diagrams, proportional to $n_i u_1^3$ or $(n_i u_0^2)^{248}$, which is not mentioned in this work. Hopefully we can discuss more about how they affect these geometric quantities. On the other hand, there are also other interactions, such as electron-electron⁵¹ or electron-phonon⁵² interactions, can also be studied according to Eqs. (4)-(7). Moreover, herein we just applied this theory to a two-band graphene, a linear approximation Dirac model. In the future, we will consider the effect of impurities scattering in the twist graphene^{27,28}, which might be more conducive to explore the contribution of disorder scattering.

It is well known one can obtain the effect of disorder on BC by measuring quantum anomalous Hall conductivity⁴, which is the integral of BC immediately. Although QM is of equal importance, it has been less explored until now. Generally speaking, as an intermediate physical quantity of multiple coefficients, including intrinsic nonlinear Hall conductivity^{14,43}, orbital magnetic susceptibilities⁵³, flat-band superconductivity²⁷, linear displacement current⁵⁴, QM is difficult to measure directly due to being coupled with other complex functions. But there have been continuous efforts to measure QM directly in different systems^{55,56}. Thus, it is expected that our results may be explained by experiments to prove the effect of disorder on QM.

ACKNOWLEDGMENTS

This work is supported in part by the Training Program of Major Research plan of the National Natural Science Foundation of China (Grant No. 92165105), and CAS Project for Young Scientists in Basic Research-Grant No. YSBR-057, the NSFC (Grant No. 11974348 and No. 11834014), and the Strategic Priority Research Program of CAS (Grant No. XDB28000000 and No. XDB33000000).

Appendix A: The summation on Matsubara frequencies in Feynman diagrams

For the diagram (iii) in Fig. 1, we get

$$S_{\mathbf{k}\mathbf{k}',\text{iii}}(\omega) = \frac{1}{\beta} \sum_{\mathbf{k}''} \langle V_{\mathbf{k}''\mathbf{k}}^{++} V_{\mathbf{k}\mathbf{k}''}^{+-} \rangle \sum_{ip} G_{\mathbf{k}}^{R,+}(ip+i\omega) G_{\mathbf{k}'}^{R,+}(ip+i\omega) G_{\mathbf{k}'}^{A,-}(ip) G_{\mathbf{k}}^{A,+}(ip), \quad (\text{A1})$$

where $G_{\mathbf{k}}^{R/A}$ is the retarded (advanced) Green's function.

Firstly, we calculate the sum of Green's functions^{46,57},

$$\begin{aligned}
I_{\mathbf{k}\mathbf{k}',\text{iii}}(\omega) &= \frac{1}{\beta} \sum_{ip} G_{\mathbf{k}}^{R,+} (ip + i\omega) G_{\mathbf{k}'}^{R,+} (ip + i\omega) G_{\mathbf{k}'}^{A,-} (ip) G_{\mathbf{k}}^{A,+} (ip) = \frac{1}{\beta} \sum_{ip} \frac{1}{ip + i\omega - \varepsilon_{\mathbf{k}}^+} \frac{1}{ip + i\omega - \varepsilon_{\mathbf{k}'}^+} \frac{1}{ip - \varepsilon_{\mathbf{k}'}^-} \frac{1}{ip - \varepsilon_{\mathbf{k}}^+} \\
&= f(\varepsilon_{\mathbf{k}}^+) \frac{1}{\varepsilon_{\mathbf{k}}^+ - \varepsilon_{\mathbf{k}'}^+} \frac{1}{i\omega + \varepsilon_{\mathbf{k}'}^- - \varepsilon_{\mathbf{k}}^+} \frac{1}{i\omega} + f(\varepsilon_{\mathbf{k}'}^+) \frac{1}{\varepsilon_{\mathbf{k}'}^+ - \varepsilon_{\mathbf{k}}^+} \frac{1}{i\omega + \varepsilon_{\mathbf{k}}^- - \varepsilon_{\mathbf{k}'}^+} \frac{1}{i\omega + \varepsilon_{\mathbf{k}}^+ - \varepsilon_{\mathbf{k}'}^+} \\
&\quad + f(\varepsilon_{\mathbf{k}}^-) \frac{1}{\varepsilon_{\mathbf{k}}^- - \varepsilon_{\mathbf{k}'}^+} \frac{1}{i\omega + \varepsilon_{\mathbf{k}'}^- - \varepsilon_{\mathbf{k}}^+} \frac{1}{i\omega + \varepsilon_{\mathbf{k}'}^- - \varepsilon_{\mathbf{k}}^+} + f(\varepsilon_{\mathbf{k}'}^-) \frac{1}{\varepsilon_{\mathbf{k}}^+ - \varepsilon_{\mathbf{k}'}^-} \frac{1}{i\omega + \varepsilon_{\mathbf{k}}^+ - \varepsilon_{\mathbf{k}'}^-} \frac{1}{i\omega} \\
&\xrightarrow{i\omega \rightarrow \omega + i\eta} \frac{f(\varepsilon_{\mathbf{k}}^+)}{\varepsilon_{\mathbf{k}}^+ - \varepsilon_{\mathbf{k}'}^+} \frac{1}{\varepsilon_{\mathbf{k}'}^- - \varepsilon_{\mathbf{k}}^+ + \omega + i\eta} \frac{1}{\omega + i\eta} + \frac{f(\varepsilon_{\mathbf{k}'}^+)}{\varepsilon_{\mathbf{k}'}^+ - \varepsilon_{\mathbf{k}}^+} \frac{1}{\varepsilon_{\mathbf{k}}^- - \varepsilon_{\mathbf{k}'}^+ + \omega + i\eta} \frac{1}{\varepsilon_{\mathbf{k}}^+ - \varepsilon_{\mathbf{k}'}^+ + \omega + i\eta} \\
&\quad + \frac{f(\varepsilon_{\mathbf{k}}^-)}{\varepsilon_{\mathbf{k}}^- + \omega + i\eta - \varepsilon_{\mathbf{k}}^+} \frac{1}{\varepsilon_{\mathbf{k}'}^- + \omega + i\eta - \varepsilon_{\mathbf{k}}^+} \frac{1}{\varepsilon_{\mathbf{k}'}^- - \varepsilon_{\mathbf{k}}^+} + \frac{f(\varepsilon_{\mathbf{k}'}^-)}{\omega + i\eta} \frac{1}{\varepsilon_{\mathbf{k}}^+ + \omega + i\eta - \varepsilon_{\mathbf{k}'}^-} \frac{1}{\varepsilon_{\mathbf{k}}^+ - \varepsilon_{\mathbf{k}'}^-} \\
&= \frac{f(\varepsilon_{\mathbf{k}}^+)}{\varepsilon_{\mathbf{k}}^+ - \varepsilon_{\mathbf{k}'}^+} \left[\frac{1}{\omega + \varepsilon_{\mathbf{k}'}^- - \varepsilon_{\mathbf{k}}^+} - i\pi\delta(\omega + \varepsilon_{\mathbf{k}'}^- - \varepsilon_{\mathbf{k}}^+) \right] \left[\frac{1}{\omega} - i\pi\delta(\omega) \right] \\
&\quad + \frac{f(\varepsilon_{\mathbf{k}'}^+)}{\varepsilon_{\mathbf{k}}^+ - \varepsilon_{\mathbf{k}'}^+} \left[\frac{1}{\omega + \varepsilon_{\mathbf{k}}^- - \varepsilon_{\mathbf{k}'}^+} - i\pi\delta(\omega + \varepsilon_{\mathbf{k}}^- - \varepsilon_{\mathbf{k}'}^+) \right] \left[\frac{1}{\omega + \varepsilon_{\mathbf{k}}^+ - \varepsilon_{\mathbf{k}'}^+} - i\pi\delta(\omega + \varepsilon_{\mathbf{k}}^+ - \varepsilon_{\mathbf{k}'}^+) \right] \\
&\quad + \frac{f(\varepsilon_{\mathbf{k}}^-)}{\varepsilon_{\mathbf{k}'}^- - \varepsilon_{\mathbf{k}}^+} \left[\frac{1}{\omega + \varepsilon_{\mathbf{k}'}^- - \varepsilon_{\mathbf{k}}^+} - i\pi\delta(\omega + \varepsilon_{\mathbf{k}'}^- - \varepsilon_{\mathbf{k}}^+) \right] \left[\frac{1}{\omega + \varepsilon_{\mathbf{k}'}^- - \varepsilon_{\mathbf{k}}^+} - i\pi\delta(\omega + \varepsilon_{\mathbf{k}'}^- - \varepsilon_{\mathbf{k}}^+) \right] \\
&\quad + \frac{f(\varepsilon_{\mathbf{k}'}^-)}{\varepsilon_{\mathbf{k}}^+ - \varepsilon_{\mathbf{k}'}^-} \left[\frac{1}{\omega + \varepsilon_{\mathbf{k}}^+ - \varepsilon_{\mathbf{k}'}^-} - i\pi\delta(\omega + \varepsilon_{\mathbf{k}}^+ - \varepsilon_{\mathbf{k}'}^-) \right] \left[\frac{1}{\omega} - i\pi\delta(\omega) \right].
\end{aligned} \tag{A2}$$

Appendix B: Some calculations in two-band gapped graphene

1. Impurity average

The Hamiltonian for two-band gapped graphene is

$$H = \begin{bmatrix} \frac{\Delta}{2} & v_D \hbar (\tau k_x - i k_y) \\ v_D \hbar (\tau k_x + i k_y) & -\frac{\Delta}{2} \end{bmatrix}, \tag{B1}$$

Let $K_1 = \tau v_D \hbar k_x$, $K_2 = v_D \hbar k_y$, $K_3 = \frac{\Delta}{2}$, $K = \sqrt{K_1^2 + K_2^2 + K_3^2}$, $\tan \varphi = \frac{K_2}{K_1}$, $\cos \theta = \frac{K_3}{K}$, $a = \sqrt{\frac{1 + \cos \theta}{2}}$, $b = \sqrt{\frac{1 - \cos \theta}{2}}$. Thus, the wave function can be written as

$$\begin{aligned}
|+\rangle &= \begin{pmatrix} K + K_3 \\ K_1 + iK_2 \end{pmatrix} = \begin{pmatrix} a \\ be^{i\varphi} \end{pmatrix}, \\
|-\rangle &= \begin{pmatrix} -K + K_3 \\ K_1 + iK_2 \end{pmatrix} = \begin{pmatrix} -b \\ ae^{i\varphi} \end{pmatrix},
\end{aligned} \tag{B2}$$

where the + and - indicate the upper and lower energy band. The Berry connection for inter and intraband are

$$\begin{aligned}
A_{x/y}^{+-} &= \langle + | i\partial_{x/y} | - \rangle = \frac{\tau v_D^2 \hbar^2 k_{y/x} - i \frac{\Delta}{2} v_D^2 \hbar^2 k_{x/y} / K}{2 \sin \theta K^2}, \\
A_{x/y}^{++} &= \langle + | i\partial_{x/y} | + \rangle = \frac{\tau v_D^2 \hbar^2 k_{y/x}}{2K(K + \frac{\Delta}{2})}.
\end{aligned} \tag{B3}$$

Considering the impurity average, $V_{\mathbf{k}\mathbf{k}'}^{++}$ can be written as⁴⁸

$$\begin{aligned}
V_{\mathbf{k}\mathbf{k}'}^{++} &= \langle +, \mathbf{k} | V(r) | +, \mathbf{k}' \rangle \\
&= \int dr (a, be^{-i\varphi}) e^{-i\mathbf{k}r} \sigma_0 \sum_i u_i \delta(r - R_i) \begin{pmatrix} a' \\ b' e^{i\varphi'} \end{pmatrix} e^{i\mathbf{k}'r} \\
&= \sum_i u_i e^{i(\mathbf{k}' - \mathbf{k})R_i} [aa' + bb' e^{i(\varphi' - \varphi)}].
\end{aligned} \tag{B4}$$

And

$$\langle V_{\mathbf{k}\mathbf{k}'}^{++} V_{\mathbf{k}'\mathbf{k}}^{++} \rangle_{\text{imp}} = n_i u_0^2 [a^2 a'^2 + b^2 b'^2 + 2aa'bb' \cos(\varphi' - \varphi)], \tag{B5}$$

where a', b', φ' are all dependent on the \mathbf{k}' .

2. Self-energy and relaxation time

According to the Dyson equation for $\mathcal{G}_{\mathbf{k}} = \frac{1}{ip - \varepsilon_{\mathbf{k}} - \Sigma_{\mathbf{k}}}$, we have

$$\begin{aligned}
\langle \varphi, \mathbf{k} | V(r) | \varphi, \mathbf{k}' \rangle &= \begin{pmatrix} V^{++} & V^{+-} \\ V^{-+} & V^{--} \end{pmatrix} \\
&= \begin{pmatrix} a^2 + b^2 e^{i(\varphi' - \varphi)} & -ab + abe^{i(\varphi' - \varphi)} \\ -ab + abe^{i(\varphi' - \varphi)} & b^2 + a^2 e^{i(\varphi' - \varphi)} \end{pmatrix}.
\end{aligned} \tag{B6}$$

Considering the impurity average, Green's function become diagonal with respect to the band index in eigen-

state representation,

$$\langle \varphi, \mathbf{k}' | G_{\mathbf{k}} | \varphi, \mathbf{k}' \rangle = \begin{pmatrix} G_{\mathbf{k}}^+ & 0 \\ 0 & G_{\mathbf{k}}^- \end{pmatrix} = \begin{pmatrix} \frac{1}{ip - \varepsilon_{\mathbf{k}}} & 0 \\ 0 & \frac{1}{ip + \varepsilon_{\mathbf{k}}} \end{pmatrix}. \quad (\text{B7})$$

Because the translation invariant is recovered after the impurity average, Σ become diagonal with respect to the wave vector. Thus

$$\Sigma = \langle VGV \rangle = \begin{pmatrix} \Sigma^+ & 0 \\ 0 & \Sigma^- \end{pmatrix}, \quad (\text{B8})$$

where

$$\begin{aligned} \Sigma^{\pm} &= \langle V_{\mathbf{k}\mathbf{k}'}^{\pm\pm} V_{\mathbf{k}'\mathbf{k}}^{\pm\pm} \rangle_{\text{imp}} G_{\mathbf{k}}^+ + \langle V_{\mathbf{k}\mathbf{k}'}^{\pm\mp} V_{\mathbf{k}'\mathbf{k}}^{\mp\pm} \rangle_{\text{imp}} G_{\mathbf{k}}^- \\ &= -\frac{n_i u_0^2 L^2}{4\pi v_D^2 \hbar^2} (\varepsilon_{\mathbf{k}}^{\pm} \pm \frac{\Delta^2}{4\varepsilon_{\mathbf{k}}}) \ln \left(\frac{\varepsilon_{\mathbf{k}}^{\pm 2} - \varepsilon_c^2}{\varepsilon_{\mathbf{k}}^{\pm 2}} \right). \end{aligned} \quad (\text{B9})$$

Then we obtain

$$\begin{aligned} \Sigma^{\pm} &= -\frac{n_i u_0^2 L^2}{4\pi v_D^2 \hbar^2} (\varepsilon_{\mathbf{k}}^{\pm} \pm \frac{\Delta^2}{4\varepsilon_{\mathbf{k}}^{\pm}}) (\ln \left| \frac{\varepsilon_{\mathbf{k}}^{\pm 2} - \varepsilon_c^2}{\varepsilon_{\mathbf{k}}^{\pm 2}} \right| + i\pi), \\ \frac{1}{\tau_{\mathbf{k}}^+} &= -\frac{2}{\hbar} \text{Im} \Sigma_{\mathbf{k}}^+ = \frac{n_i u_0^2 L^2}{2\hbar v_D^2 \hbar^2} (\varepsilon_{\mathbf{k}}^+ + \frac{\Delta^2}{4\varepsilon_{\mathbf{k}}^+}). \end{aligned} \quad (\text{B10})$$

3. The corrected vertices

Take the $\tilde{\mathcal{A}}_{x,\mathbf{k}}^{+-}(\omega)$ as an example. In the weak disorder limit and $\varepsilon \ll \hbar\omega$ we have⁴³

$$\mathcal{G}_{\mathbf{k}}^R(\varepsilon + \hbar\omega) \mathcal{G}_{\mathbf{k}}^A(\varepsilon) \approx \frac{2\pi}{\hbar} \frac{\tau_{\mathbf{k}}}{1 - i\frac{\omega}{\hbar}\tau_{\mathbf{k}}} \delta(\varepsilon - \varepsilon_{\mathbf{k}}), \quad (\text{B11})$$

then,

$$\begin{aligned} \tilde{\mathcal{A}}_{x,\mathbf{k}}^{+-}(\omega) &= \mathcal{A}_{\mu\mathbf{k}}^{++} + \sum_{\mathbf{k}''} \langle V_{\mathbf{k}''\mathbf{k}}^{++} V_{\mathbf{k}\mathbf{k}''}^{++} \rangle \mathcal{G}_{\mathbf{k}''}^{R,+} \mathcal{G}_{\mathbf{k}''}^{A,+} \tilde{\mathcal{A}}_{x,\mathbf{k}''}^{+-}(\omega) \\ &\approx \mathcal{A}_{x\mathbf{k}}^{++} + \frac{n_i u_0^2 L^2}{(2\pi)^2} \int \mathbf{k}'' d\mathbf{k}'' \int d\varphi'' [a^2 a''^2 + b^2 b''^2 + 2aa''bb'' \cos(\varphi'' - \varphi)] \frac{2\pi}{\hbar} \frac{\tau_{\mathbf{k}''}^+}{1 - i\frac{\omega}{\hbar}\tau_{\mathbf{k}''}^+} \delta(\varepsilon - \varepsilon_{\mathbf{k}''}^+) \tilde{\mathcal{A}}_{x,\mathbf{k}''}^{+-}(\omega) \\ &= \frac{\tau v_D \hbar \sin \theta \sin \varphi}{2(\varepsilon_{\mathbf{k}}^+ + \frac{\Delta}{2})} + \frac{n_i u_0^2 L^2}{2\hbar} \int \mathbf{k}'' d\mathbf{k}'' 2aa''bb'' \frac{\tau_{\mathbf{k}''}^+}{1 - i\frac{\omega}{\hbar}\tau_{\mathbf{k}''}^+} \delta(\varepsilon_{\mathbf{k}}^+ - \varepsilon_{\mathbf{k}''}^+) \tilde{\mathcal{A}}_{x,\mathbf{k}''}^{+-}(\omega) \\ &= \frac{\tau v_D \hbar \sin \theta \sin \varphi}{2(\varepsilon_{\mathbf{k}}^+ + \frac{\Delta}{2})} + \frac{n_i u_0^2 L^2}{4\hbar v_D^2 \hbar^2} \varepsilon_{\mathbf{k}}^+ \sin^2 \theta \frac{\tau_{\mathbf{k}}^+}{1 - i\frac{\omega}{\hbar}\tau_{\mathbf{k}}^+} \tilde{\mathcal{A}}_{x,\mathbf{k}}^{+-}(\omega). \end{aligned} \quad (\text{B12})$$

And

$$\begin{aligned} \tilde{\mathcal{A}}_{x,\mathbf{k}}^{++}(\omega) &= \frac{1 - B + \frac{\omega^2}{\hbar^2} \tau_{\mathbf{k}}^{+2} + i\frac{\omega}{\hbar} \tau_{\mathbf{k}}^+ B}{(1 - B)^2 + \frac{\omega^2}{\hbar^2} \tau_{\mathbf{k}}^{+2}} \mathcal{A}_{x\mathbf{k}}^{++}, \\ \tilde{\mathcal{A}}_{y,\mathbf{k}}^{++}(\omega) &= \frac{1 - B + \frac{\omega^2}{\hbar^2} \tau_{\mathbf{k}}^{+2} + i\frac{\omega}{\hbar} \tau_{\mathbf{k}}^+ B}{(1 - B)^2 + \frac{\omega^2}{\hbar^2} \tau_{\mathbf{k}}^{+2}} \mathcal{A}_{y\mathbf{k}}^{++}, \end{aligned} \quad (\text{B13})$$

where $B = \frac{n_i u_0^2 L^2}{4\hbar^3 v_D^2} \varepsilon_{\mathbf{k}}^+ \sin^2 \theta \tau_{\mathbf{k}}^+$ and $L = 1\text{\AA}$.

4. The calculations of dressed BC and QM

According to Eq. (8), for the diagram (iii) we can get

$$\chi_{xy,\mathbf{k},\text{iii}}^+ = \sum_{\mathbf{k}'} \int_0^{\infty} \tilde{\mathcal{A}}_{x,\mathbf{k}}^{++}(\omega) \mathcal{A}_{y,\mathbf{k}'}^{+-} S_{\mathbf{k}\mathbf{k}',\text{iii}}(\omega) d\omega = \sum_{\mathbf{k}'} \mathcal{A}_{y,\mathbf{k}'}^{+-} \int_0^{\infty} \tilde{\mathcal{A}}_{x,\mathbf{k}}^{++}(\omega) S_{\mathbf{k}\mathbf{k}',\text{iii}}(\omega) d\omega. \quad (\text{B14})$$

Considering the reciprocity of integration and summation, we deal with the integral part first,

$$\chi_{xy,\mathbf{k},\text{iii}}^+ = \sum_{\mathbf{k}'} \mathcal{A}_{y,\mathbf{k}'}^{+-} \langle V_{\mathbf{k}\mathbf{k}'}^{++} V_{\mathbf{k}'\mathbf{k}}^{--} \rangle \int_0^{\infty} \tilde{\mathcal{A}}_{x,\mathbf{k}}^{++}(\omega) I_{\mathbf{k}\mathbf{k}',\text{iii}}(\omega) d\omega, \quad (\text{B15})$$

where

$$\begin{aligned}
& \int_0^\infty \tilde{\mathcal{A}}_{x,\mathbf{k}}^{++}(\omega) I_{\mathbf{k}\mathbf{k}',\text{iii}}(\omega) d\omega = \frac{f(\varepsilon_{\mathbf{k}}^+)}{\varepsilon_{\mathbf{k}}^+ - \varepsilon_{\mathbf{k}'}^+} \int_0^\infty \tilde{\mathcal{A}}_{x,\mathbf{k}}^{++}(\omega) \left[\frac{-i\pi\delta(\omega)}{\omega + \varepsilon_{\mathbf{k}'}^- - \varepsilon_{\mathbf{k}}^+} + \frac{-i\pi\delta(\omega + \varepsilon_{\mathbf{k}'}^- - \varepsilon_{\mathbf{k}}^+)}{\omega} - \pi^2\delta(\omega + \varepsilon_{\mathbf{k}'}^- - \varepsilon_{\mathbf{k}}^+) \delta(\omega) \right] \\
& + \frac{f(\varepsilon_{\mathbf{k}'}^+)}{\varepsilon_{\mathbf{k}}^+ - \varepsilon_{\mathbf{k}'}^+} \int_0^\infty \tilde{\mathcal{A}}_{x,\mathbf{k}}^{++}(\omega) \left[\frac{-i\pi\delta(\omega + \varepsilon_{\mathbf{k}}^+ - \varepsilon_{\mathbf{k}'}^+)}{\omega + \varepsilon_{\mathbf{k}}^- - \varepsilon_{\mathbf{k}'}^+} + \frac{-i\pi\delta(\omega + \varepsilon_{\mathbf{k}}^- - \varepsilon_{\mathbf{k}'}^+)}{\omega + \varepsilon_{\mathbf{k}}^+ - \varepsilon_{\mathbf{k}'}^+} - \pi^2\delta(\omega + \varepsilon_{\mathbf{k}}^- - \varepsilon_{\mathbf{k}'}^+) \delta(\omega + \varepsilon_{\mathbf{k}}^+ - \varepsilon_{\mathbf{k}'}^+) \right] \\
& + \frac{f(\varepsilon_{\mathbf{k}}^-)}{\varepsilon_{\mathbf{k}}^- - \varepsilon_{\mathbf{k}}^+} \int_0^\infty \tilde{\mathcal{A}}_{x,\mathbf{k}}^{++}(\omega) \left[\frac{-i\pi\delta(\omega + \varepsilon_{\mathbf{k}}^- - \varepsilon_{\mathbf{k}}^+)}{\omega + \varepsilon_{\mathbf{k}}^- - \varepsilon_{\mathbf{k}}^+} + \frac{-i\pi\delta(\omega + \varepsilon_{\mathbf{k}}^- - \varepsilon_{\mathbf{k}}^+)}{\omega + \varepsilon_{\mathbf{k}}^- - \varepsilon_{\mathbf{k}}^+} - \pi^2\delta(\omega + \varepsilon_{\mathbf{k}}^- - \varepsilon_{\mathbf{k}}^+) \delta(\omega + \varepsilon_{\mathbf{k}}^- - \varepsilon_{\mathbf{k}}^+) \right] \\
& + \frac{f(\varepsilon_{\mathbf{k}}^+)}{\varepsilon_{\mathbf{k}}^+ - \varepsilon_{\mathbf{k}}^-} \int_0^\infty \tilde{\mathcal{A}}_{x,\mathbf{k}}^{++}(\omega) \left[\frac{-i\pi\delta(\omega)}{\omega + \varepsilon_{\mathbf{k}}^+ - \varepsilon_{\mathbf{k}}^-} + \frac{-i\pi\delta(\omega + \varepsilon_{\mathbf{k}}^+ - \varepsilon_{\mathbf{k}}^-)}{\omega} - \pi^2\delta(\omega + \varepsilon_{\mathbf{k}}^+ - \varepsilon_{\mathbf{k}}^-) \delta(\omega) \right] \\
& = -i\pi \tilde{\mathcal{A}}_{x,\mathbf{k}}^{++}(\omega) \left[\frac{f(\varepsilon_{\mathbf{k}}^+) - f(\varepsilon_{\mathbf{k}}^-)}{(\varepsilon_{\mathbf{k}}^+ - \varepsilon_{\mathbf{k}}^+) (\varepsilon_{\mathbf{k}}^+ - \varepsilon_{\mathbf{k}}^-)} \right] \Big|_{\omega=\varepsilon_{\mathbf{k}}^+ - \varepsilon_{\mathbf{k}}^-} > 0} - i\pi \tilde{\mathcal{A}}_{x,\mathbf{k}}^{++}(\omega) \left[\frac{f(\varepsilon_{\mathbf{k}'}^+) - f(\varepsilon_{\mathbf{k}}^+)}{(\varepsilon_{\mathbf{k}}^+ - \varepsilon_{\mathbf{k}'}^+) (\varepsilon_{\mathbf{k}}^+ - \varepsilon_{\mathbf{k}}^-)} \right] \Big|_{\omega=\varepsilon_{\mathbf{k}}^+ - \varepsilon_{\mathbf{k}'}^+} > 0} \\
& - i\pi \tilde{\mathcal{A}}_{x,\mathbf{k}}^{++}(\omega) \left[\frac{f(\varepsilon_{\mathbf{k}}^-) - f(\varepsilon_{\mathbf{k}}^+)}{(\varepsilon_{\mathbf{k}}^+ - \varepsilon_{\mathbf{k}}^+) (\varepsilon_{\mathbf{k}}^+ - \varepsilon_{\mathbf{k}}^-)} \right] \Big|_{\omega=\varepsilon_{\mathbf{k}}^- - \varepsilon_{\mathbf{k}}^+} > 0} - \pi^2 \left[f(\varepsilon_{\mathbf{k}}^+) \tilde{\mathcal{A}}_{x,\mathbf{k}}^{++}(\omega) \Big|_{\omega=0}^\delta - f(\varepsilon_{\mathbf{k}}^-) \tilde{\mathcal{A}}_{x,\mathbf{k}}^{++}(\omega) \Big|_{\omega=\varepsilon_{\mathbf{k}}^+ - \varepsilon_{\mathbf{k}}^-} \right] \frac{\delta(\varepsilon_{\mathbf{k}}^+ - \varepsilon_{\mathbf{k}}^+)}{\varepsilon_{\mathbf{k}}^+ - \varepsilon_{\mathbf{k}}^-}. \tag{B16}
\end{aligned}$$

Next, we plan to calculate the susceptibility for the diagram (iii) in Fig. 1,

$$\begin{aligned}
\chi_{xy,\mathbf{k},\text{iii}}^+ &= \sum_{\mathbf{k}'} \mathcal{A}_{y,\mathbf{k}'}^{+-} \langle V_{\mathbf{k}\mathbf{k}'}^{++} V_{\mathbf{k}'\mathbf{k}}^{-+} \rangle \int_0^\infty \tilde{\mathcal{A}}_{x,\mathbf{k}}^{++}(\omega) I_{\mathbf{k}\mathbf{k}',1}(\omega) d\omega \\
&= \frac{L^2}{(2\pi)^2} \int \mathbf{k}' d\mathbf{k}' \int d\varphi' \frac{-v_D \hbar \varepsilon_{\mathbf{k}'}^+ \cos \varphi' - i \frac{\Delta}{2} v_D \sin \varphi'}{2\varepsilon_{\mathbf{k}'}^{+2}} n_i u_0^2 [a'b^2b' - a^2a'b' + aa'^2be^{i(\varphi-\varphi')} - abb'^2e^{i(\varphi'-\varphi)}] \\
& \left\{ -i\pi \tilde{\mathcal{A}}_{x,\mathbf{k}}^{++}(\omega) \left[\frac{f(\varepsilon_{\mathbf{k}}^+) - f(\varepsilon_{\mathbf{k}'}^-)}{(\varepsilon_{\mathbf{k}}^+ - \varepsilon_{\mathbf{k}'}^+) (\varepsilon_{\mathbf{k}}^+ - \varepsilon_{\mathbf{k}}^-)} \right] \Big|_{\omega=\varepsilon_{\mathbf{k}}^+ - \varepsilon_{\mathbf{k}'}^-} > 0} - i\pi \tilde{\mathcal{A}}_{x,\mathbf{k}}^{++}(\omega) \left[\frac{f(\varepsilon_{\mathbf{k}'}^+) - f(\varepsilon_{\mathbf{k}}^+)}{(\varepsilon_{\mathbf{k}}^+ - \varepsilon_{\mathbf{k}'}^+) (\varepsilon_{\mathbf{k}}^+ - \varepsilon_{\mathbf{k}}^-)} \right] \Big|_{\omega=\varepsilon_{\mathbf{k}}^+ - \varepsilon_{\mathbf{k}'}^+} > 0} \right. \\
& - i\pi \tilde{\mathcal{A}}_{x,\mathbf{k}}^{++}(\omega) \left[\frac{f(\varepsilon_{\mathbf{k}}^-) - f(\varepsilon_{\mathbf{k}}^+)}{(\varepsilon_{\mathbf{k}}^+ - \varepsilon_{\mathbf{k}}^+) (\varepsilon_{\mathbf{k}}^+ - \varepsilon_{\mathbf{k}}^-)} \right] \Big|_{\omega=\varepsilon_{\mathbf{k}}^- - \varepsilon_{\mathbf{k}}^+} > 0} \\
& \left. - \pi^2 \left[f(\varepsilon_{\mathbf{k}}^+) \tilde{\mathcal{A}}_{x,\mathbf{k}}^{++}(\omega) \Big|_{\omega=0}^\delta - f(\varepsilon_{\mathbf{k}}^-) \tilde{\mathcal{A}}_{x,\mathbf{k}}^{++}(\omega) \Big|_{\omega=\varepsilon_{\mathbf{k}}^+ - \varepsilon_{\mathbf{k}}^-} \right] \frac{\delta(\varepsilon_{\mathbf{k}}^+ - \varepsilon_{\mathbf{k}}^+)}{\varepsilon_{\mathbf{k}}^+ - \varepsilon_{\mathbf{k}}^-} \right\}. \tag{B17}
\end{aligned}$$

As we know, at zero temperature limit we have

$$f(\varepsilon_{\mathbf{k}}^+) - f(\varepsilon_{\mathbf{k}'}^+) \approx f'(\varepsilon_{\mathbf{k}}^+) (\varepsilon_{\mathbf{k}}^+ - \varepsilon_{\mathbf{k}'}^+) \approx -\delta(\varepsilon_{\mathbf{k}}^+ - \varepsilon_{\mathbf{k}}^+) (\varepsilon_{\mathbf{k}}^+ - \varepsilon_{\mathbf{k}'}^+). \tag{B18}$$

Thus, we obtain

$$\begin{aligned}
\chi_{xy,\mathbf{k},\text{iii}}^+ &= -\frac{iabn_i u_0^2 L^2}{8\hbar v_D} \frac{-\varepsilon_f \Delta \cos \varphi - i \left[\varepsilon_f^2 + \left(\frac{\Delta}{2}\right)^2 \right] \sin \varphi}{\varepsilon_f^2} \tilde{\mathcal{A}}_{x\mathbf{k}}^{++}(\omega) \Big|_{\omega=\varepsilon_f - \varepsilon_{\mathbf{k}}^+} > 0} \\
& - \frac{\pi abn_i u_0^2 L^2}{16\hbar v_D} \frac{-\varepsilon_{\mathbf{k}}^+ \Delta \cos \varphi - i \left[\varepsilon_f^2 + \left(\frac{\Delta}{2}\right)^2 \right] \sin \varphi}{\varepsilon_{\mathbf{k}}^{+3}} \left[\tilde{\mathcal{A}}_{x\mathbf{k}}^{++}(\omega) f(\varepsilon_{\mathbf{k}}^+) \Big|_{\omega=0} - \tilde{\mathcal{A}}_{x\mathbf{k}}^{++}(\omega) f(-\varepsilon_{\mathbf{k}}^+) \Big|_{\omega=\varepsilon_{\mathbf{k}}^+ + \varepsilon_f} > 0} \right]. \tag{B19}
\end{aligned}$$

Other three diagrams for + band are

$$\begin{aligned}
\chi_{xy,\mathbf{k},\text{iv}}^+ &= -\frac{i\tau abn_i u_0^2 L^2 \left(\varepsilon_f^2 + \frac{\Delta^2}{4}\right) i \cos \varphi + \varepsilon_f \Delta \sin \varphi}{8\hbar v_D \varepsilon_f^2} \frac{\tilde{\mathcal{A}}_{y\mathbf{k}}^{+++}(\omega)}{\varepsilon_{\mathbf{k}}^+ + \varepsilon_f} \Big|_{\omega=\varepsilon_f - \varepsilon_{\mathbf{k}}^+ > 0} \\
&\quad - \frac{\pi\tau abn_i u_0^2 L^2 \left(\varepsilon_f^2 + \frac{\Delta^2}{4}\right) i \cos \varphi + \varepsilon_{\mathbf{k}}^+ \Delta \sin \varphi}{16\hbar v_D \varepsilon_{\mathbf{k}}^{+3}} [f(a) - f(-a)] \tilde{\mathcal{A}}_{y\mathbf{k}}^{+++}(\omega) \Big|_{\omega=\varepsilon_f - \varepsilon_{\mathbf{k}}^+ > 0}, \\
\chi_{xy,\mathbf{k},\text{v}}^+ &= -\frac{iabn_i u_0^2 L^2 - \varepsilon_{\mathbf{k}}^+ \frac{\Delta}{2} \cos \varphi - i\left(\frac{\Delta}{2}\right)^2 \sin \varphi}{4\hbar v_D \varepsilon_{\mathbf{k}}^{+2}} \frac{\tilde{\mathcal{A}}_{x\mathbf{k}}^{+++}(\omega)}{\varepsilon_{\mathbf{k}}^+ + \varepsilon_f} \Big|_{\omega=\varepsilon_{\mathbf{k}}^+ - \varepsilon_f > 0} \\
&\quad + \frac{\pi v_D abn_i u_0^2 L^2 - \varepsilon_{\mathbf{k}}^+ \frac{\Delta}{2} \cos \varphi - i\left(\frac{\Delta}{2}\right)^2 \sin \varphi}{8\hbar^2 v_D^2 \varepsilon_{\mathbf{k}}^{+3}} \tilde{\mathcal{A}}_{y\mathbf{k}}^{+++}(\omega) f(\varepsilon_{\mathbf{k}}^+) \Big|_{\omega=0}, \\
\chi_{xy,\mathbf{k},\text{vi}}^+ &= -\frac{i\tau abn_i u_0^2 L^2 \varepsilon_{\mathbf{k}}^+ \frac{\Delta}{2} \sin \varphi + i\left(\frac{\Delta}{2}\right)^2 \cos \varphi}{4\hbar v_D \varepsilon_{\mathbf{k}}^{+2}} \frac{\tilde{\mathcal{A}}_{x\mathbf{k}}^{+++}(\omega)}{\varepsilon_{\mathbf{k}}^+ + \varepsilon_f} \Big|_{\omega=\varepsilon_{\mathbf{k}}^+ - \varepsilon_f > 0} \\
&\quad + \frac{\tau\pi abn_i u_0^2 L^2 \varepsilon_{\mathbf{k}}^+ \frac{\Delta}{2} \sin \varphi + i\left(\frac{\Delta}{2}\right)^2 \cos \varphi}{8\hbar^2 v_D^2 \varepsilon_{\mathbf{k}}^{+2}} \tilde{\mathcal{A}}_{y\mathbf{k}}^{+++}(\omega) f(\varepsilon_{\mathbf{k}}^+) \Big|_{\omega=0}.
\end{aligned} \tag{B20}$$

According to the Fig. 1, the (vii)-(ix) diagrams are for - band,

$$\begin{aligned}
\chi_{xy,\mathbf{k},\text{vii}}^- &= \frac{ivabn_i u_0^2 L^2 - \varepsilon_f \Delta \cos \varphi + \left(\varepsilon_f^2 + \frac{\Delta^2}{4}\right) i \sin \varphi}{8\hbar v_D \varepsilon_f^2} \frac{\tilde{\mathcal{A}}_{x\mathbf{k}}^{+++}(\omega)}{\varepsilon_{\mathbf{k}}^+ + \varepsilon_f} \Big|_{\omega=\varepsilon_{\mathbf{k}}^+ - \varepsilon_f > 0} \\
&\quad - \frac{\pi abn_i u_0^2 L^2 - \varepsilon_{\mathbf{k}}^+ \Delta \cos \varphi + \left(\varepsilon_{\mathbf{k}}^{+2} + \frac{\Delta^2}{4}\right) i \sin \varphi}{16\hbar v_D \varepsilon_{\mathbf{k}}^{+3}} \tilde{\mathcal{A}}_{x\mathbf{k}}^{+++}(\omega) f(\varepsilon_{\mathbf{k}}^+) \Big|_{\omega=0}, \\
\chi_{xy,\mathbf{k},\text{viii}}^- &= \frac{i\tau abn_i u_0^2 L^2 - \left(\varepsilon_f^2 + \frac{\Delta^2}{4}\right) i \cos \varphi + \varepsilon_f \Delta \sin \varphi}{8\hbar v_D \varepsilon_f^2} \frac{\tilde{\mathcal{A}}_{y\mathbf{k}}^{+++}(\omega)}{\varepsilon_{\mathbf{k}}^+ + \varepsilon_f} \Big|_{\omega=\varepsilon_{\mathbf{k}}^+ - \varepsilon_f > 0} \\
&\quad - \frac{\pi\tau abn_i u_0^2 L^2 - \left(\varepsilon_{\mathbf{k}}^{+2} + \frac{\Delta^2}{4}\right) i \cos \varphi + \varepsilon_{\mathbf{k}}^+ \Delta \sin \varphi}{16\hbar v_D \varepsilon_{\mathbf{k}}^{+3}} f(\varepsilon_a) \tilde{\mathcal{A}}_{y\mathbf{k}}^{+++}(\omega) \Big|_{\omega=0}, \\
\chi_{xy,\mathbf{k},\text{ix}}^- &= \frac{iabn_i u_0^2 L^2 - \varepsilon_{\mathbf{k}}^+ \frac{\Delta}{2} \cos \varphi + i\left(\frac{\Delta}{2}\right)^2 \sin \varphi}{4\hbar v_D \varepsilon_{\mathbf{k}}^{+2}} \frac{\tilde{\mathcal{A}}_{x\mathbf{k}}^{+++}(\omega)}{\varepsilon_{\mathbf{k}}^+ + \varepsilon_f} \Big|_{\omega=\varepsilon_f - \varepsilon_{\mathbf{k}}^+ > 0} \\
&\quad + \frac{\pi v_D abn_i u_0^2 L^2 - \varepsilon_{\mathbf{k}}^+ \frac{\Delta}{2} \cos \varphi + i\left(\frac{\Delta}{2}\right)^2 \sin \varphi}{8\hbar^2 v_D^2 \varepsilon_{\mathbf{k}}^{+3}} \tilde{\mathcal{A}}_{x\mathbf{k}}^{+++}(\omega) f(\varepsilon_{\mathbf{k}}^+) \Big|_{\omega=0}, \\
\chi_{xy,\mathbf{k},\text{x}}^- &= \frac{i\tau abn_i u_0^2 L^2 \varepsilon_{\mathbf{k}}^+ \frac{\Delta}{2} \sin \varphi - i\left(\frac{\Delta}{2}\right)^2 \cos \varphi}{4\hbar v_D \varepsilon_{\mathbf{k}}^{+2}} \frac{\tilde{\mathcal{A}}_{x\mathbf{k}}^{+++}(\omega)}{\varepsilon_f + \varepsilon_{\mathbf{k}}^+} \Big|_{\omega=\varepsilon_f - \varepsilon_{\mathbf{k}}^+ > 0} \\
&\quad + \frac{\tau\pi abn_i u_0^2 L^2 \varepsilon_{\mathbf{k}}^+ \frac{\Delta}{2} \sin \varphi - i\left(\frac{\Delta}{2}\right)^2 \cos \varphi}{8\hbar^2 v_D^2 \varepsilon_{\mathbf{k}}^{+2}} \tilde{\mathcal{A}}_{y\mathbf{k}}^{+++}(\omega) f(\varepsilon_{\mathbf{k}}^+) \Big|_{\omega=0}.
\end{aligned} \tag{B21}$$

5. The dressed DC and QM

The diagonal dressed Berry curvature and quantum metric for \pm band are written as

$$\begin{aligned}
g_{xy,\mathbf{k}}^{d,+}/\Omega_{xy,\mathbf{k}}^{d,+} &= -\frac{1}{2\pi}\text{Im} \times / -\frac{1}{\pi}\text{Re} \times \\
\frac{\sin \theta n_i u_0^2 L^2}{8v_D \hbar} &\left\{ \frac{i}{2} \frac{-\varepsilon_f^+ \frac{\Delta}{2} \cos \varphi + \varepsilon_f^2 i \sin \varphi - \varepsilon_f \frac{\Delta}{2} \cos \varphi + (\frac{\Delta}{2})^2 i \sin \varphi}{\varepsilon_f^{+2}} \frac{\tilde{\mathcal{A}}_{x\mathbf{k}}^{+++}(\omega)}{\varepsilon_{\mathbf{k}}^+ + \varepsilon_f} \Big|_{\omega=\varepsilon_{\mathbf{k}}^+ - \varepsilon_f > 0} \right. \\
&- \frac{\pi}{4} \frac{-\varepsilon_{\mathbf{k}}^+ \frac{\Delta}{2} \cos \varphi + \varepsilon_{\mathbf{k}}^{+2} i \sin \varphi - \varepsilon_{\mathbf{k}}^+ \frac{\Delta}{2} \cos \varphi + (\frac{\Delta}{2})^2 i \sin \varphi}{\varepsilon_{\mathbf{k}}^{+3}} f(\varepsilon_{\mathbf{k}}^+) \tilde{\mathcal{A}}_{x\mathbf{k}}^{+++}(\omega) \Big|_{\omega=0} \\
&+ \frac{i\tau}{2} \frac{-\varepsilon_f^2 i \cos \varphi + \varepsilon_f \frac{\Delta}{2} \sin \varphi + \varepsilon_f \frac{\Delta}{2} \sin \varphi - (\frac{\Delta}{2})^2 i \cos \varphi}{\varepsilon_f^{+2}} \frac{\tilde{\mathcal{A}}_{y\mathbf{k}}^{+++}(\omega)}{\varepsilon_{\mathbf{k}}^+ + \varepsilon_f} \Big|_{\omega=\varepsilon_{\mathbf{k}}^+ - \varepsilon_f > 0} \\
&- \frac{\pi\tau}{4} \frac{-\varepsilon_{\mathbf{k}}^{+2} i \cos \varphi + \varepsilon_{\mathbf{k}}^+ \frac{\Delta}{2} \sin \varphi + \varepsilon_{\mathbf{k}}^+ \frac{\Delta}{2} \sin \varphi - (\frac{\Delta}{2})^2 i \cos \varphi}{\varepsilon_{\mathbf{k}}^{+3}} f(\varepsilon_{\mathbf{k}}^+) \tilde{\mathcal{A}}_{y\mathbf{k}}^{+++}(\omega) \Big|_{\omega=0} \\
&+ i \frac{-\varepsilon_{\mathbf{k}}^+ \frac{\Delta}{2} \cos \varphi + i(\frac{\Delta}{2})^2 \sin \varphi}{\varepsilon_{\mathbf{k}}^{+2}} \frac{\tilde{\mathcal{A}}_{x\mathbf{k}}^{+++}(\omega)}{\varepsilon_{\mathbf{k}}^+ + \varepsilon_f^+} \Big|_{\omega=\varepsilon_f - \varepsilon_{\mathbf{k}}^+ > 0} + \frac{\pi}{2} \frac{-\varepsilon_{\mathbf{k}}^+ \frac{\Delta}{2} \cos \varphi + i(\frac{\Delta}{2})^2 \sin \varphi}{\varepsilon_{\mathbf{k}}^{+3}} f(\varepsilon_{\mathbf{k}}^+) \tilde{\mathcal{A}}_{x\mathbf{k}}^{+++}(\omega) \Big|_{\omega=0} \\
&+ i\tau \frac{\varepsilon_{\mathbf{k}}^+ \frac{\Delta}{2} \sin \varphi - i(\frac{\Delta}{2})^2 \cos \varphi}{\varepsilon_{\mathbf{k}}^{+2}} \frac{\tilde{\mathcal{A}}_{y\mathbf{k}}^{+++}(\omega)}{\varepsilon_f + \varepsilon_{\mathbf{k}}^+} \Big|_{\omega=\varepsilon_f - \varepsilon_{\mathbf{k}}^+ > 0} + \frac{\tau\pi}{2} \frac{\varepsilon_{\mathbf{k}}^+ \frac{\Delta}{2} \sin \varphi - i(\frac{\Delta}{2})^2 \cos \varphi}{\varepsilon_{\mathbf{k}}^{+3}} f(\varepsilon_{\mathbf{k}}^+) \tilde{\mathcal{A}}_{y\mathbf{k}}^{+++}(\omega) \Big|_{\omega=0} \\
&\pm \frac{i\tau}{2} \frac{\varepsilon_f^2 i \cos \varphi + \varepsilon_f^+ \frac{\Delta}{2} \sin \varphi + (\frac{\Delta}{2})^2 i \cos \varphi + \varepsilon_f \frac{\Delta}{2} \sin \varphi}{\varepsilon_f^{+2}} \frac{\tilde{\mathcal{A}}_{y\mathbf{k}}^{+++}(\omega)}{\varepsilon_{\mathbf{k}}^+ + \varepsilon_f} \Big|_{\omega=\varepsilon_{\mathbf{k}}^+ - \varepsilon_f > 0} \\
&\mp \frac{\pi\tau}{4} \frac{\varepsilon_{\mathbf{k}}^{+2} i \cos \varphi + \varepsilon_{\mathbf{k}}^+ \frac{\Delta}{2} \sin \varphi + (\frac{\Delta}{2})^2 i \cos \varphi + \varepsilon_{\mathbf{k}}^+ \frac{\Delta}{2} \sin \varphi}{\varepsilon_{\mathbf{k}}^{+3}} f(\varepsilon_{\mathbf{k}}^+) \tilde{\mathcal{A}}_{y\mathbf{k}}^{+++}(\omega) \Big|_{\omega=0} \\
&\pm \frac{i}{2} \frac{-\varepsilon_f^2 i \sin \varphi - \varepsilon_f \frac{\Delta}{2} \cos \varphi - \varepsilon_f \frac{\Delta}{2} \cos \varphi - (\frac{\Delta}{2})^2 i \sin \varphi}{\varepsilon_f^{+2}} \frac{\tilde{\mathcal{A}}_{x\mathbf{k}}^{+++}(\omega)}{\varepsilon_{\mathbf{k}}^+ + \varepsilon_f} \Big|_{\omega=\varepsilon_{\mathbf{k}}^+ - \varepsilon_f > 0} \\
&\mp \frac{\pi}{4} \frac{-\varepsilon_{\mathbf{k}}^{+2} i \sin \varphi - \varepsilon_{\mathbf{k}}^+ \frac{\Delta}{2} \cos \varphi - \varepsilon_{\mathbf{k}}^+ \frac{\Delta}{2} \cos \varphi - (\frac{\Delta}{2})^2 i \sin \varphi}{\varepsilon_{\mathbf{k}}^{+3}} f(\varepsilon_{\mathbf{k}}^+) \tilde{\mathcal{A}}_{x\mathbf{k}}^{+++}(\omega) \Big|_{\omega=0} \\
&\pm i\tau \frac{\varepsilon_{\mathbf{k}}^+ \frac{\Delta}{2} \sin \varphi + i(\frac{\Delta}{2})^2 \cos \varphi}{\varepsilon_{\mathbf{k}}^{+2}} \frac{\tilde{\mathcal{A}}_{y\mathbf{k}}^{+++}(\omega)}{\varepsilon_{\mathbf{k}}^+ + \varepsilon_f^+} \Big|_{\omega=\varepsilon_f - \varepsilon_{\mathbf{k}}^+ > 0} + \frac{\tau\pi}{2} \frac{\varepsilon_{\mathbf{k}}^+ \frac{\Delta}{2} \sin \varphi + i(\frac{\Delta}{2})^2 \cos \varphi}{\varepsilon_{\mathbf{k}}^{+3}} f(\varepsilon_{\mathbf{k}}^+) \tilde{\mathcal{A}}_{y\mathbf{k}}^{+++}(\omega) \Big|_{\omega=0} \\
&\pm i \frac{-\varepsilon_{\mathbf{k}}^+ \frac{\Delta}{2} \cos \varphi - i(\frac{\Delta}{2})^2 \sin \varphi}{\varepsilon_{\mathbf{k}}^{+2}} \frac{\tilde{\mathcal{A}}_{x\mathbf{k}}^{+++}(\omega)}{\varepsilon_f + \varepsilon_{\mathbf{k}}^+} \Big|_{\omega=\varepsilon_f - \varepsilon_{\mathbf{k}}^+ > 0} + \frac{\pi}{2} \frac{-\varepsilon_{\mathbf{k}}^+ \frac{\Delta}{2} \cos \varphi - i(\frac{\Delta}{2})^2 \sin \varphi}{\varepsilon_{\mathbf{k}}^{+3}} f(\varepsilon_{\mathbf{k}}^+) \tilde{\mathcal{A}}_{x\mathbf{k}}^{+++}(\omega) \Big|_{\omega=0} \left. \right\} \tag{B22}
\end{aligned}$$

$$\begin{aligned}
& g_{xy,\mathbf{k}}^{d,-}/\Omega_{xy,\mathbf{k}}^{d,-} = -\frac{1}{2\pi}\text{Im} \times / -\frac{1}{\pi}\text{Re} \times \\
& \frac{\sin \theta n_i u_0^2 L^2}{8v_D \hbar} \left\{ \begin{aligned}
& -\frac{i - \varepsilon_f \frac{\Delta}{2} \cos \varphi - \varepsilon_f^{+2} i \sin \varphi - \varepsilon_f \frac{\Delta}{2} \cos \varphi - (\frac{\Delta}{2})^2 i \sin \varphi}{\varepsilon_f^{+2}} \frac{\tilde{\mathcal{A}}_{x\mathbf{k}}^{++}(\omega)}{\varepsilon_{\mathbf{k}}^+ + \varepsilon_f} \Big|_{\omega=\varepsilon_f - \varepsilon_{\mathbf{k}}^+ > 0} \\
& -\frac{\pi - \varepsilon_{\mathbf{k}}^+ \frac{\Delta}{2} \cos \varphi - \varepsilon_{\mathbf{k}}^{+2} i \sin \varphi - \varepsilon_{\mathbf{k}}^+ \frac{\Delta}{2} \cos \varphi - (\frac{\Delta}{2})^2 i \sin \varphi}{\varepsilon_{\mathbf{k}}^{+3}} \tilde{\mathcal{A}}_{x\mathbf{k}}^{++}(\omega) \left[f(\varepsilon_{\mathbf{k}}^+) \Big|_{\omega=0} - f(-\varepsilon_{\mathbf{k}}^+) \Big|_{\omega=\varepsilon_{\mathbf{k}}^+ + \varepsilon_f} \right] \\
& -\frac{i\tau \varepsilon_f^{+2} i \cos \varphi + \varepsilon_f \frac{\Delta}{2} \sin \varphi + \varepsilon_f \frac{\Delta}{2} \sin \varphi + (\frac{\Delta}{2})^2 i \cos \varphi}{\varepsilon_f^{+2}} \frac{\tilde{\mathcal{A}}_{y\mathbf{k}}^{++}(\omega)}{\varepsilon_{\mathbf{k}}^+ + \varepsilon_f} \Big|_{\omega=\varepsilon_f - \varepsilon_{\mathbf{k}}^+ > 0} \\
& -\frac{\pi\tau \varepsilon_{\mathbf{k}}^{+2} i \cos \varphi + \varepsilon_{\mathbf{k}}^+ \frac{\Delta}{2} \sin \varphi + \varepsilon_{\mathbf{k}}^+ \frac{\Delta}{2} \sin \varphi + (\frac{\Delta}{2})^2 i \cos \varphi}{\varepsilon_{\mathbf{k}}^{+3}} \tilde{\mathcal{A}}_{y\mathbf{k}}^{++}(\omega) \left[f(\varepsilon_{\mathbf{k}}^+) \Big|_{\omega=0} - f(-\varepsilon_{\mathbf{k}}^+) \Big|_{\omega=\varepsilon_{\mathbf{k}}^+ + \varepsilon_f} \right] \\
& -i \frac{-\varepsilon_{\mathbf{k}}^+ \frac{\Delta}{2} \cos \varphi - i(\frac{\Delta}{2})^2 \sin \varphi}{\varepsilon_{\mathbf{k}}^{+2}} \frac{\tilde{\mathcal{A}}_{x\mathbf{k}}^{++}(\omega)}{\varepsilon_{\mathbf{k}}^+ + \varepsilon_f} \Big|_{\omega=\varepsilon_{\mathbf{k}}^+ - \varepsilon_f > 0} + \frac{\pi - \varepsilon_{\mathbf{k}}^+ \frac{\Delta}{2} \cos \varphi - i(\frac{\Delta}{2})^2 \sin \varphi}{\varepsilon_{\mathbf{k}}^{+3}} f(\varepsilon_{\mathbf{k}}^+) \tilde{\mathcal{A}}_{x\mathbf{k}}^{++}(\omega) \Big|_{\omega=0} \\
& -i\tau \frac{\varepsilon_{\mathbf{k}}^+ \frac{\Delta}{2} \sin \varphi + i(\frac{\Delta}{2})^2 \cos \varphi}{\varepsilon_{\mathbf{k}}^{+2}} \frac{\tilde{\mathcal{A}}_{y\mathbf{k}}^{++}(\omega)}{\varepsilon_f + \varepsilon_{\mathbf{k}}^+} \Big|_{\omega=\varepsilon_{\mathbf{k}}^+ - \varepsilon_f > 0} + \frac{\pi\tau \varepsilon_{\mathbf{k}}^+ \frac{\Delta}{2} \sin \varphi + i(\frac{\Delta}{2})^2 \cos \varphi}{\varepsilon_{\mathbf{k}}^{+3}} f(\varepsilon_{\mathbf{k}}^+) \tilde{\mathcal{A}}_{y\mathbf{k}}^{++}(\omega) \Big|_{\omega=0} \\
& \mp \frac{i\tau - \varepsilon_f^{+2} i \cos \varphi + \varepsilon_f \frac{\Delta}{2} \sin \varphi - (\frac{\Delta}{2})^2 i \cos \varphi + \varepsilon_f \frac{\Delta}{2} \sin \varphi}{\varepsilon_f^{+2}} \frac{\tilde{\mathcal{A}}_{y\mathbf{k}}^{++}(\omega)}{\varepsilon_{\mathbf{k}}^+ + \varepsilon_f} \Big|_{\omega=\varepsilon_f - \varepsilon_{\mathbf{k}}^+ > 0} \\
& \mp \frac{\pi\tau - \varepsilon_{\mathbf{k}}^{+2} i \cos \varphi + \varepsilon_{\mathbf{k}}^+ \frac{\Delta}{2} \sin \varphi - (\frac{\Delta}{2})^2 i \cos \varphi + \varepsilon_{\mathbf{k}}^+ \frac{\Delta}{2} \sin \varphi}{\varepsilon_{\mathbf{k}}^{+3}} \tilde{\mathcal{A}}_{y\mathbf{k}}^{++}(\omega) \left[f(\varepsilon_{\mathbf{k}}^+) \Big|_{\omega=0} - f(-\varepsilon_{\mathbf{k}}^+) \Big|_{\omega=\varepsilon_{\mathbf{k}}^+ + \varepsilon_f} \right] \\
& \mp \frac{i \varepsilon_f^{+2} i \sin \varphi - \varepsilon_f \frac{\Delta}{2} \cos \varphi - \varepsilon_f \frac{\Delta}{2} \cos \varphi + (\frac{\Delta}{2})^2 i \sin \varphi}{\varepsilon_f^{+2}} \frac{\tilde{\mathcal{A}}_{x\mathbf{k}}^{++}(\omega)}{\varepsilon_{\mathbf{k}}^+ + \varepsilon_f} \Big|_{\omega=\varepsilon_f - \varepsilon_{\mathbf{k}}^+ > 0} \\
& \mp \frac{\pi \varepsilon_{\mathbf{k}}^{+2} i \sin \varphi - \varepsilon_{\mathbf{k}}^+ \frac{\Delta}{2} \cos \varphi - \varepsilon_{\mathbf{k}}^+ \frac{\Delta}{2} \cos \varphi + (\frac{\Delta}{2})^2 i \sin \varphi}{\varepsilon_{\mathbf{k}}^{+3}} \tilde{\mathcal{A}}_{x\mathbf{k}}^{++}(\omega) \left[f(\varepsilon_{\mathbf{k}}^+) \Big|_{\omega=0} - f(-\varepsilon_{\mathbf{k}}^+) \Big|_{\omega=\varepsilon_{\mathbf{k}}^+ + \varepsilon_f} \right] \\
& \mp i\tau \frac{\varepsilon_{\mathbf{k}}^+ \frac{\Delta}{2} \sin \varphi - i(\frac{\Delta}{2})^2 \cos \varphi}{\varepsilon_{\mathbf{k}}^{+2}} \frac{\tilde{\mathcal{A}}_{y\mathbf{k}}^{++}(\omega)}{\varepsilon_{\mathbf{k}}^+ + \varepsilon_f} \Big|_{\omega=\varepsilon_{\mathbf{k}}^+ - \varepsilon_f > 0} + \frac{\pi\tau \varepsilon_{\mathbf{k}}^+ \frac{\Delta}{2} \sin \varphi - i(\frac{\Delta}{2})^2 \cos \varphi}{\varepsilon_{\mathbf{k}}^{+3}} f(\varepsilon_{\mathbf{k}}^+) \tilde{\mathcal{A}}_{y\mathbf{k}}^{++}(\omega) \Big|_{\omega=0} \\
& \mp i \frac{-\varepsilon_{\mathbf{k}}^+ \frac{\Delta}{2} \cos \varphi + i(\frac{\Delta}{2})^2 \sin \varphi}{\varepsilon_{\mathbf{k}}^{+2}} \frac{\tilde{\mathcal{A}}_{x\mathbf{k}}^{++}(\omega)}{\varepsilon_f + \varepsilon_{\mathbf{k}}^+} \Big|_{\omega=\varepsilon_{\mathbf{k}}^+ - \varepsilon_f > 0} + \frac{\pi - \varepsilon_{\mathbf{k}}^+ \frac{\Delta}{2} \cos \varphi + i(\frac{\Delta}{2})^2 \sin \varphi}{\varepsilon_{\mathbf{k}}^{+3}} f(\varepsilon_{\mathbf{k}}^+) \tilde{\mathcal{A}}_{x\mathbf{k}}^{++}(\omega) \Big|_{\omega=0} \end{aligned} \right\} \tag{B23}
\end{aligned}$$

* The authors contribute equally.

† zgzhu@ucas.ac.cn

‡ gsu@ucas.ac.cn

¹ J. P. Provost and G. Vallee, *Commun. Math. Phys.* **76**, 289 (1980).

² M. V. Berry, *Proc. R. Soc. A* **392**, 45 (1984).

³ M. V. Berry, *J. Phys. A: Math. Gen.* **18**, 15 (1985).

⁴ D. Xiao, M.-C. Chang, and Q. Niu, *Rev. Mod. Phys.* **82**, 1959 (2010).

⁵ S. Q. Shen, *Topological Insulators-Dirac Equation in Condensed Matter, 2nd edition* (Springer, New York, 2017).

⁶ D. J. Thouless, M. Kohmoto, M. P. Nightingale, and M. den Nijs, *Phys. Rev. Lett.* **49**, 405 (1982).

⁷ M. Z. Hasan and C. L. Kane, *Rev. Mod. Phys.* **82**, 3045 (2010).

⁸ X.-L. Qi and S.-C. Zhang, *Rev. Mod. Phys.* **83**, 1057

(2011).

⁹ L. Fu and C. L. Kane, *Phys. Rev. B* **74**, 195312 (2006).

¹⁰ L. Fu, C. L. Kane, and E. J. Mele, *Phys. Rev. Lett.* **98**, 106803 (2007).

¹¹ I. Sodemann and L. Fu, *Phys. Rev. Lett.* **115**, 216806 (2015).

¹² C.-P. Zhang, X.-J. Gao, Y.-M. Xie, H. C. Po, and K. T. Law, *Phys. Rev. B* **107**, 115142 (2023).

¹³ Y. Gao, *Front Phys* **14**, 33404 (2019).

¹⁴ C. Ortix, *Adv. Quantum Technol.* **4**, 2100056 (2021).

¹⁵ S. Saha and A. Narayan, *J. Phys.: Condens. Matter* **35**, 485301 (2023).

¹⁶ T.-Y. Zhao, A.-Q. Wang, X.-G. Ye, X.-Y. Liu, X. Liao, and Z.-M. Liao, *Phys. Rev. Lett.* **131**, 186302 (2023).

¹⁷ T. Nishijima, T. Watanabe, H. Sekiguchi, Y. Ando, E. Shigematsu, R. Ohshima, S. Kuroda, and M. Shiraiishi,

- Nano Lett. **23**, 2247 (2023).
- ¹⁸ Z.-F. Zhang, Z.-G. Zhu, and G. Su, *Phys. Rev. B* **104**, 115140 (2021).
- ¹⁹ Y. Wang, Z.-G. Zhu, and G. Su, *Phys. Rev. B* **106**, 035148 (2022).
- ²⁰ Z.-F. Zhang, Z.-G. Zhu, and G. Su, *Natl. Sci. Rev.* **10**, nwad104 (2023).
- ²¹ D. Chruściński and A. Jamiolkowski, “Geometry of quantum evolution,” in *Geometric Phases in Classical and Quantum Mechanics* (Birkhäuser Boston, 2004) pp. 179–238.
- ²² R. Resta, *Eur. Phys. J. B* **79**, 121 (2011).
- ²³ J. A. Austrich-Olivares and J. D. Vergara, *Entropy* **24**, 1236 (2022).
- ²⁴ D. Gonzalez, D. Gutiérrez-Ruiz, and J. D. Vergara, *Phys. Rev. E* **99**, 032144 (2019).
- ²⁵ S. B. Juárez, D. Gonzalez, D. Gutiérrez-Ruiz, and J. D. Vergara, *Phys. Scr.* **98**, 095106 (2023).
- ²⁶ H.-T. Ding, Y.-Q. Zhu, P. He, Y.-G. Liu, J.-T. Wang, D.-W. Zhang, and S.-L. Zhu, *Phys. Rev. A* **105**, 012210 (2022).
- ²⁷ S. A. Chen and K. Law, *Phys. Rev. Lett.* **132**, 026002 (2024).
- ²⁸ T. B. Smith, L. Pullasserri, and A. Srivastava, *Phys. Rev. Research* **4**, 013217 (2022).
- ²⁹ F. Piéchon, A. Raoux, J.-N. Fuchs, and G. Montambaux, *Phys. Rev. B* **94**, 134423 (2016).
- ³⁰ G. Palumbo and N. Goldman, *Phys. Rev. Lett.* **121**, 170401 (2018).
- ³¹ T. Ozawa and B. Mera, *Phys. Rev. B* **104**, 045103 (2021).
- ³² Y. Wang, Z.-G. Zhu, and G. Su, *Phys. Rev. Research* **5**, 043156 (2023).
- ³³ Y. Wang, Z. Zhang, Z.-G. Zhu, and G. Su, *Phys. Rev. B* **109**, 085419 (2024).
- ³⁴ A. Gao, Y.-F. Liu, J.-X. Qiu, B. Ghosh, T. V. Trevisan, Y. Onishi, C. Hu, T. Qian, H.-J. Tien, S.-W. Chen, M. Huang, D. Bérubé, H. Li, C. Tzschaschel, T. Dinh, Z. Sun, S.-C. Ho, S.-W. Lien, B. Singh, K. Watanabe, T. Taniguchi, D. C. Bell, H. Lin, T.-R. Chang, C. R. Du, A. Bansil, L. Fu, N. Ni, P. P. Orth, Q. Ma, and S.-Y. Xu, *Science* **381**, 181 (2023).
- ³⁵ N. Wang, D. Kaplan, Z. Zhang, T. Holder, N. Cao, A. Wang, X. Zhou, F. Zhou, Z. Jiang, C. Zhang, S. Ru, H. Cai, K. Watanabe, T. Taniguchi, B. Yan, and W. Gao, *Nature* **621**, 487 (2023).
- ³⁶ K. Das, S. Lahiri, R. B. Atencia, D. Culcer, and A. Agarwal, *Phys. Rev. B* **108**, 1201405 (2023).
- ³⁷ W. Chen and G. von Gersdorff, *SciPost Physics Core* **5**, 040 (2022).
- ³⁸ E. R. Mucciolo and C. H. Lewenkopf, *J. Phys.: Condens. Matter* **22**, 273201 (2010).
- ³⁹ T. Vojta and F. Epperlein, *Ann. Phys. (Berlin)* **510**, 493 (1998).
- ⁴⁰ Z. Wang, H. Guo, and K. H. Bevan, *J. Comput. Electron.* **12**, 104 (2013).
- ⁴¹ B. Y.-K. Hu, E. H. Hwang, and S. Das Sarma, *Phys. Rev. B* **78**, 165411 (2008).
- ⁴² Z. Z. Du, C. M. Wang, S. Li, H.-Z. Lu, and X. C. Xie, *Nat Commun* **10**, 3047 (2019).
- ⁴³ Z. Z. Du, C. M. Wang, H.-P. Sun, H.-Z. Lu, and X. C. Xie, *Nat Commun* **12**, 5038 (2021).
- ⁴⁴ R. B. Atencia, D. Xiao, and D. Culcer, *Phys. Rev. B* **108**, 1201115 (2023).
- ⁴⁵ X.-B. Qiang, Z. Z. Du, H.-Z. Lu, and X. C. Xie, *Phys. Rev. B* **107**, 1161302 (2023).
- ⁴⁶ H. Bruss and K. Flensberg, *Introduction to many body quantum theory in condensed matter physics*, edited by online (Oxford University Press, 2003).
- ⁴⁷ G. D. Mahan, *Many-Particle Physics* (Springer, Berlin, 2013).
- ⁴⁸ N. A. Sinitsyn, A. H. MacDonald, T. Jungwirth, V. K. Dugaev, and J. Sinova, *Phys. Rev. B* **75**, 045315 (2007).
- ⁴⁹ M. Koshino and T. Ando, *Phys. Rev. B* **73**, 245403 (2006).
- ⁵⁰ A. Srivastava and A. Imamoğlu, *Phys. Rev. Lett.* **115**, 166802 (2015).
- ⁵¹ V. N. Kotov, B. Uchoa, V. M. Pereira, F. Guinea, and A. H. Castro Neto, *Rev. Mod. Phys.* **84**, 1067 (2012).
- ⁵² C.-H. Park, F. Giustino, M. L. Cohen, and S. G. Louie, *Nano Lett.* **8**, 4229 (2008).
- ⁵³ Y. Gao, S. A. Yang, and Q. Niu, *Phys. Rev. Lett.* **112**, 166601 (2014).
- ⁵⁴ L. Xiang, B. Wang, Y. Wei, Z. Qiao, and J. Wang, *Phys. Rev. B* **109**, 115121 (2024).
- ⁵⁵ M. Yu, P. Yang, M. Gong, Q. Cao, Q. Lu, H. Liu, S. Zhang, M. B. Plenio, F. Jelezko, T. Ozawa, N. Goldman, and J. Cai, *Natl. Sci. Rev.* **7**, 254 (2019).
- ⁵⁶ A. Gianfrate, O. Bleu, L. Dominici, V. Ardizzone, M. De Giorgi, D. Ballarini, G. Lerario, K. W. West, L. N. Pfeiffer, D. D. Solnyshkov, D. Sanvitto, and G. Malpuech, *Nature* **578**, 381 (2020).
- ⁵⁷ D. E. Parker, T. Morimoto, J. Orenstein, and J. E. Moore, *Phys. Rev. B* **99**, 045121 (2019).